

Control of Interacting Vortex Flows at Subsonic and Transonic Speeds Using Passive Porosity

Gary E. Erickson

NASA Langley Research Center

Mail Stop 413, Hampton, Virginia 23681, USA

Keywords: vortex flows, high angle of attack, shock waves, subsonic and transonic speeds

ABSTRACT

A wind tunnel experiment was conducted in the NASA Langley Research Center (LaRC) 8-Foot Transonic Pressure Tunnel (TPT) to determine the effects of passive surface porosity on vortex flow interactions about a general research fighter configuration at subsonic and transonic speeds. Flow-through porosity was applied to a wing leading-edge extension (LEX) mounted to a 65° cropped delta wing model to promote large nose-down pitching moment increments at high angles of attack. Porosity decreased the vorticity shed from the LEX, which weakened the LEX vortex and altered the global interactions of the LEX and wing vortices at high angles of attack. Six-component forces and moments and wing upper surface static pressure distributions were obtained at free-stream Mach numbers of 0.50, 0.85, and 1.20, Reynolds number of 2.5(10^6) per foot, angles of attack up to 30°, and angles of sideslip to +/-8°. The off-surface flow field was visualized in selected cross-planes using a laser vapor screen flow visualization technique. Test data were obtained with a centerline vertical tail and with alternate twin, wing-mounted vertical fins having 0° and 30° cant angles. In addition, the porosity of the LEX was compartmentalized to determine the sensitivity of the vortex-dominated aerodynamics to the location and level of porosity applied to the LEX.

1 INTRODUCTION

The control of leading-edge vortex flows is a continuing challenge for designers of modern fighter aircraft. Passive porosity has been successfully applied to control vortices shed from slender bodies at subsonic through supersonic speeds [1] and to mitigate the adverse effects of shock waves on wings at transonic and supersonic speeds [2, 3]. The application of porosity to control vortex interactions at supersonic speeds is summarized in [4]. The present experimental investigation focuses on flow-through porosity to affect the vortex interactions for reduced nose-up pitching moments at subsonic and transonic speeds about a 65° cropped delta wing-LEX model. Porosity was applied to the LEX, since it is situated ahead of the moment reference center and generates a strong vortex flow that affects the wing flow field. The model was tested with the non-porous (solid) LEX, porous LEX, and LEX off in combination with centerline vertical tail and twin uncanted and canted wing-mounted vertical fins. Test data were obtained at Mach=0.50, 0.85, and 1.20. Results that are presented in this paper are limited to Mach=0.85.

2 TEST INFORMATION

2.1 Model and Instrumentation

A photograph of the 65° cropped delta wing-LEX model installed in the 8-Foot TPT test section and an illustration of key dimensions of the model in terms of the fuselage station (F.S.) and butt line (B.L.) locations are included in figs. 1 and 2. The LEX was a flat-plate with beveled leading edge having a 65° sweep angle. It incorporated a pattern of 0.05-inch diameter through holes spaced 0.10 inch apart on center to provide a total porosity level of 12% relative to its exposed area. Testing of a solid LEX was accomplished by applying tape to the lower surface. An internal, 6-component strain-gauge balance was used to measure the model forces and moments. The model pitch attitude was determined using an accelerometer mounted in the main support system pitch

Report Documentation Page			Form Approved OMB No. 0704-0188	
<p>Public reporting burden for the collection of information is estimated to average 1 hour per response, including the time for reviewing instructions, searching existing data sources, gathering and maintaining the data needed, and completing and reviewing the collection of information. Send comments regarding this burden estimate or any other aspect of this collection of information, including suggestions for reducing this burden, to Washington Headquarters Services, Directorate for Information Operations and Reports, 1215 Jefferson Davis Highway, Suite 1204, Arlington VA 22202-4302. Respondents should be aware that notwithstanding any other provision of law, no person shall be subject to a penalty for failing to comply with a collection of information if it does not display a currently valid OMB control number.</p>				
1. REPORT DATE 00 MAR 2003	2. REPORT TYPE N/A	3. DATES COVERED -		
4. TITLE AND SUBTITLE Control of Interacting Vortex Flows at Subsonic and Transonic Speeds Using Passive Porosity			5a. CONTRACT NUMBER	
			5b. GRANT NUMBER	
			5c. PROGRAM ELEMENT NUMBER	
6. AUTHOR(S)			5d. PROJECT NUMBER	
			5e. TASK NUMBER	
			5f. WORK UNIT NUMBER	
7. PERFORMING ORGANIZATION NAME(S) AND ADDRESS(ES) NATO Research and Technology Organisation BP 25, 7 Rue Ancelle, F-92201 Neuilly-Sue-Seine Cedex, France			8. PERFORMING ORGANIZATION REPORT NUMBER	
9. SPONSORING/MONITORING AGENCY NAME(S) AND ADDRESS(ES)			10. SPONSOR/MONITOR'S ACRONYM(S)	
			11. SPONSOR/MONITOR'S REPORT NUMBER(S)	
12. DISTRIBUTION/AVAILABILITY STATEMENT Approved for public release, distribution unlimited				
13. SUPPLEMENTARY NOTES Also see: ADM001490, Presented at RTO Applied Vehicle Technology Panel (AVT) Symposium held in Leon, Norway on 7-11 May 2001, The original document contains color images.				
14. ABSTRACT				
15. SUBJECT TERMS				
16. SECURITY CLASSIFICATION OF: a. REPORT b. ABSTRACT c. THIS PAGE unclassified unclassified unclassified			17. LIMITATION OF ABSTRACT UU	18. NUMBER OF PAGES 8
19a. NAME OF RESPONSIBLE PERSON				

mechanism with corrections applied to account for tunnel flow angularity and aeroelastic deflections of the model/balance/sting assembly. The right-hand wing incorporated a total of 45 upper surface static pressure orifices distributed in three spanwise rows located at 30%, 60%, and 80% of the wing centerline chord measured aft from the apex of the wing (fig. 2). The pressure orifices were connected to an internal, 48-port, 15 psid electronically-scanned pressure module.

3 DISCUSSION OF RESULTS

3.1 Forces and Moments

Fig. 3 illustrates the effect of the porous LEX on the lift and pitching moment coefficients at Mach=0.85 (the LEX-off configuration is shown for reference). LEX porosity causes a slight increase in the lift at a given angle of attack compared to the solid LEX configuration. This is a surprising result considering that porosity weakens the LEX vortex. The abrupt drop-off in the lift coefficient with LEX off is associated with an interaction of the wing vortex with a normal shock wave and an associated breakdown of the vortical flow [5]. The weakening of the LEX vortex is the primary source of the large nose-down increments in the pitching moment coefficient. Porosity increases the drag (not shown) as a result of the flow through the porous surface.

Figs. 4 and 5 show the effect of LEX porosity on the variation of the rolling moment coefficient with sideslip at Mach=0.85 and $\alpha=20^\circ$ and $\alpha=24^\circ$, respectively. The solid and porous LEX configurations typically show a stable rolling moment variation with sideslip. Porosity causes a small decrease in the lateral stability at each angle of attack, and the only significant effect associated with porosity is an unstable “break” in the curve at $\beta=+/-8^\circ$ and $\alpha=24^\circ$. Off-surface flow visualization indicated an instability of the windward wing vortex system at the sideslip extremes with the porous LEX. The nonlinear rolling moment trends and marked instabilities of the LEX-off configuration are caused by the vortex-shock interaction cited in the previous paragraph.

3.2 Vapor Screen Images

Figs. 6-9 present vapor screen images with the solid LEX, porous LEX, and LEX off at Mach=0.85, the 80% wing chord station ($x/c=0.80$), and angles of attack of 16° , 20° , 24° , and 28° . This cross-plane station corresponds to the aft pressure measurement location depicted in the pressure distributions in the next section. The vapor screen images of the solid LEX configuration are characterized by distinct LEX and wing vortical flows that exhibit a strong mutual interaction, including a coiling of the vortices at the higher angles of attack. The latter effect causes the vortices to lift away from the wing upper surface, which reduces the suction pressures induced by the vortical flows [5]. LEX porosity shifts the dominance from the LEX vortex to the wing vortex. The LEX vortex is not apparent in any of the porous LEX images, which feature a single diffused, but stable, wing vortex. Porosity does not suppress the LEX vortical flow; however, it is so weak that condensate does not appear in sufficient quantity to render it visible in the vapor screen images. The porous LEX and LEX-off cross-flow patterns at a given angle of attack are similar. The most noteworthy difference, however, is that the wing vortex with LEX off is unstable at the higher angles of attack. For example, shock-induced asymmetric vortex breakdown occurs at $\alpha=24^\circ$, whereas the breakdown is symmetric at $\alpha=28^\circ$ in figs. 8 and 9, respectively. The diffused nature of the wing vortex with the porous LEX resembles a burst vortical flow, but the video tape recordings of the laser light sheet scans along the length of the wing and into the near wake indicate an unburst leading-edge vortex system. Similar flow visualization results were obtained in wind tunnel and flight testing of the F/A-18 fighter configuration, which exhibited a diffused vortex system caused by a LEX upper surface fence for high angle-of-attack vortex control [6].

3.3 Surface Static Pressure Distributions

Figs. 10-13 present representative spanwise distributions of the right-hand wing upper surface static pressure coefficient ($C_{p,u}$) plotted as a function of nondimensional span location (y/s) at $x/c=0.30$,

0.60, and $x/c=0.80$, Mach=0.85, and $\alpha=16^\circ, 20^\circ, 24^\circ$, and 28° , respectively. Results obtained with LEX off are again shown for reference. Dual vortex suction pressure signatures can be discerned in the solid LEX pressure distributions at $\alpha=16^\circ$ and $x/c=0.60$ and 0.80 in fig. 10. A single, broader vortex pressure signature with overall higher suction pressure level is apparent with the porous LEX. These trends are consistent with the vapor screen images in fig. 6, which showed a broader wing vortex situated closer to the surface with the porous LEX. The porous LEX configuration exhibits consistently higher vortex-induced suction pressure levels in comparison to the solid LEX at the higher angles of attack in figs. 11-13. These results suggest that the flow-through porosity provides an improved balance between the LEX and wing vortices at this Mach number. The wing vortex is thereby allowed to exert a greater influence on the high angle-of-attack flow field, unhindered by the direct interaction of a more dominant LEX vortical flow. The solid and porous LEX configurations retain distinct vortex pressure footprints at all measurement stations up to $\alpha=28^\circ$ since the leading-edge vortices are stable at the higher angles of attack. In contrast, the shock-induced vortex breakdown that occurs with LEX off produces markedly flatter pressure distributions and lower suction pressure levels beginning at $\alpha=24^\circ$.

SUMMARY

A wind tunnel experiment was conducted in the NASA LaRC 8-Foot TPT to determine the effects of flow-through porosity on the interacting vortex flows of a general research fighter configuration at subsonic and transonic speeds. Force, moment, and pressure measurements and laser vapor screen flow visualizations indicated that a porous LEX promoted a wing vortex-dominated flow field as a result of a diffusion and weakening of the LEX vortex. The porous LEX was effective in significantly reducing the pitching moment instability that is inherent in LEX-wing fighter configurations at high angles of attack. In addition, the increased influence of the wing vortical flow resulted in higher overall suction pressures on the wing upper surface, which countered the diminished LEX vortex-induced lift increments. Porosity effects on the rolling moment characteristics were generally limited to small decreases in the static stability level.

REFERENCES

- [1] Bauer S. X. S. and Hemsch M. J.: Alleviation of Side Force on Tangent-Ogive Forebodies Using Passive Porosity. AIAA 10th Applied Aerodynamic Conference, Palo Alto, CA, AIAA-92-2711, June 22-24, 1992.
- [2] Bauer S. X. S. and Hernandez G.: Reduction of Cross-Flow Shock-Induced Separation with a Porous Cavity at Supersonic Speeds. AIAA 6th Applied Aerodynamics Conference, Williamsburg, VA, AIAA-88-2567, June 6-8, 1988.
- [3] Hartwich P. M.: Euler Study on Porous Transonic Airfoils with a View Toward Multipoint Design. Journal of Aircraft, Vol. 30, No. 2, March-April 1993, pp. 184-191.
- [4] Erickson, G. E.: Effects of Passive Porosity on Interacting Vortex Flows at Supersonic Speeds. Presented at the 9th Millennium International Symposium on Flow Visualization, Paper No. 86, Edinburgh, Scotland, August 22-25, 2000.
- [5] Erickson, G. E.: Wind Tunnel Investigation of the Interaction and Breakdown Characteristics of Slender-Wing Vortices at Subsonic, Transonic, and Supersonic Speeds. NASA TP-3114, 1991.
- [6] Erickson, G. E.: Wind Tunnel Investigation of Vortex Flows on F/A-18 at Subsonic Through Transonic Speeds. NASA TP-3111, 1991.



model installed in NASA LaRC 8-Foot TPT

close-up view of porous LEX

Fig. 1. Photographs of porous LEX model

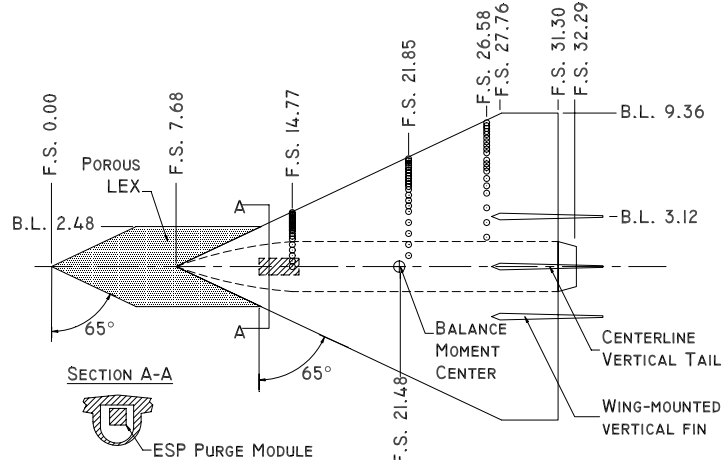


Fig. 2. Geometry details of porous LEX model

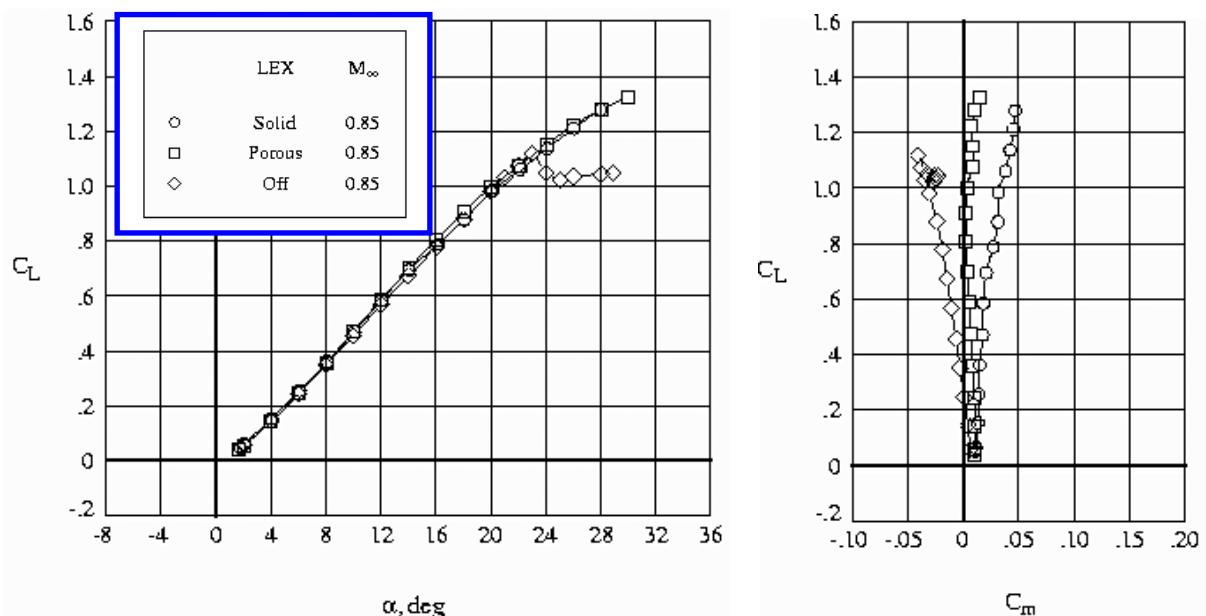


Fig. 3. Effect of LEX porosity on lift, drag, and pitching moment coefficients

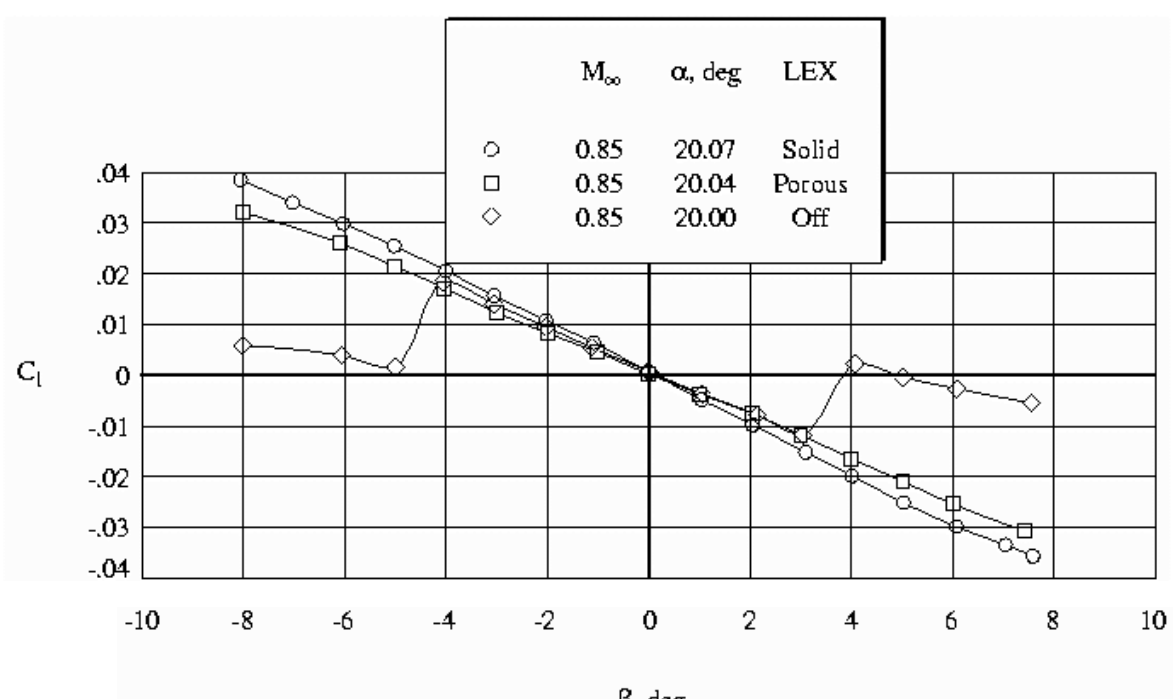


Fig. 4. Effect of LEX porosity on rolling moment coefficient versus sideslip at Mach=0.85, $\alpha=20^\circ$

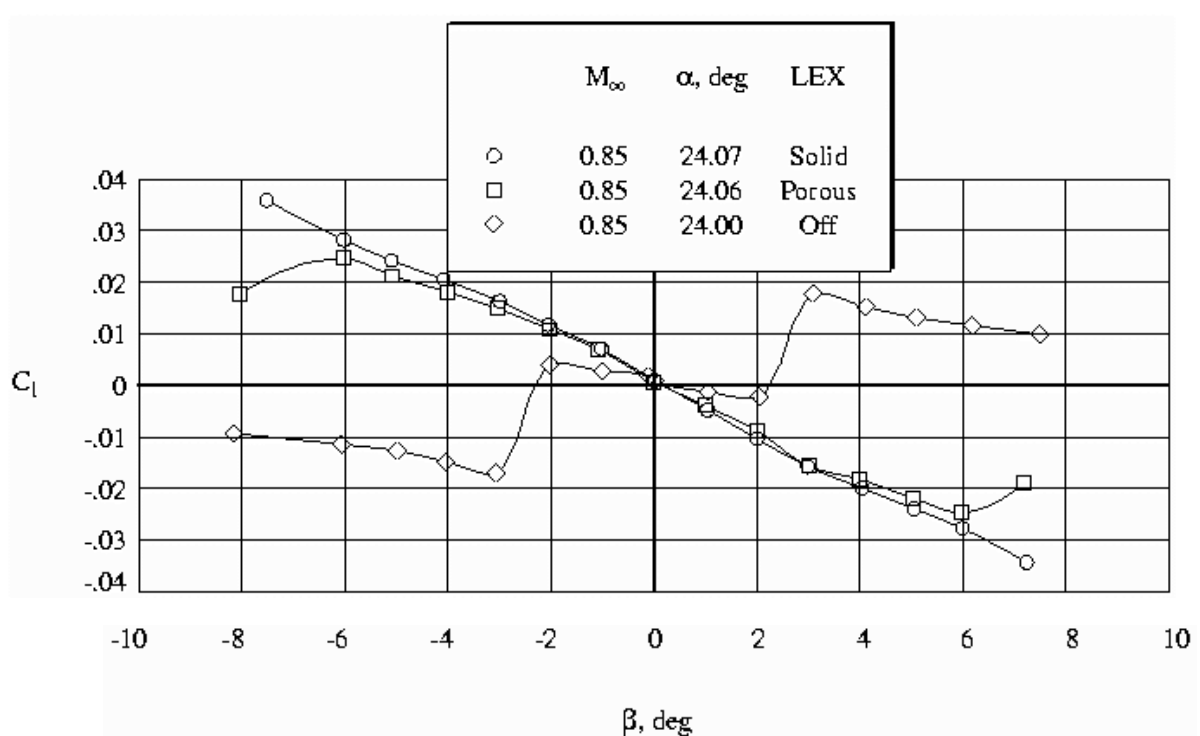


Fig. 5. Effect of LEX porosity on rolling moment coefficient versus sideslip at Mach=0.85, $\alpha=24^\circ$



Fig. 6. Laser vapor screen images at Mach=0.85 and $\alpha=16^\circ$



Fig. 7. Laser vapor screen images at Mach=0.85 and $\alpha=20^\circ$

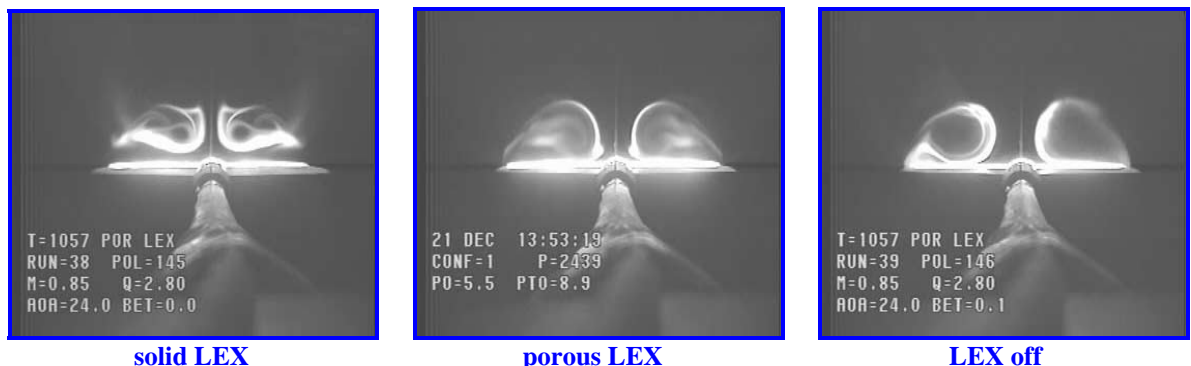


Fig. 8. Laser vapor screen images at Mach=0.85 and $\alpha=24^\circ$



Fig. 9. Laser vapor screen images at Mach=0.85 and $\alpha=28^\circ$

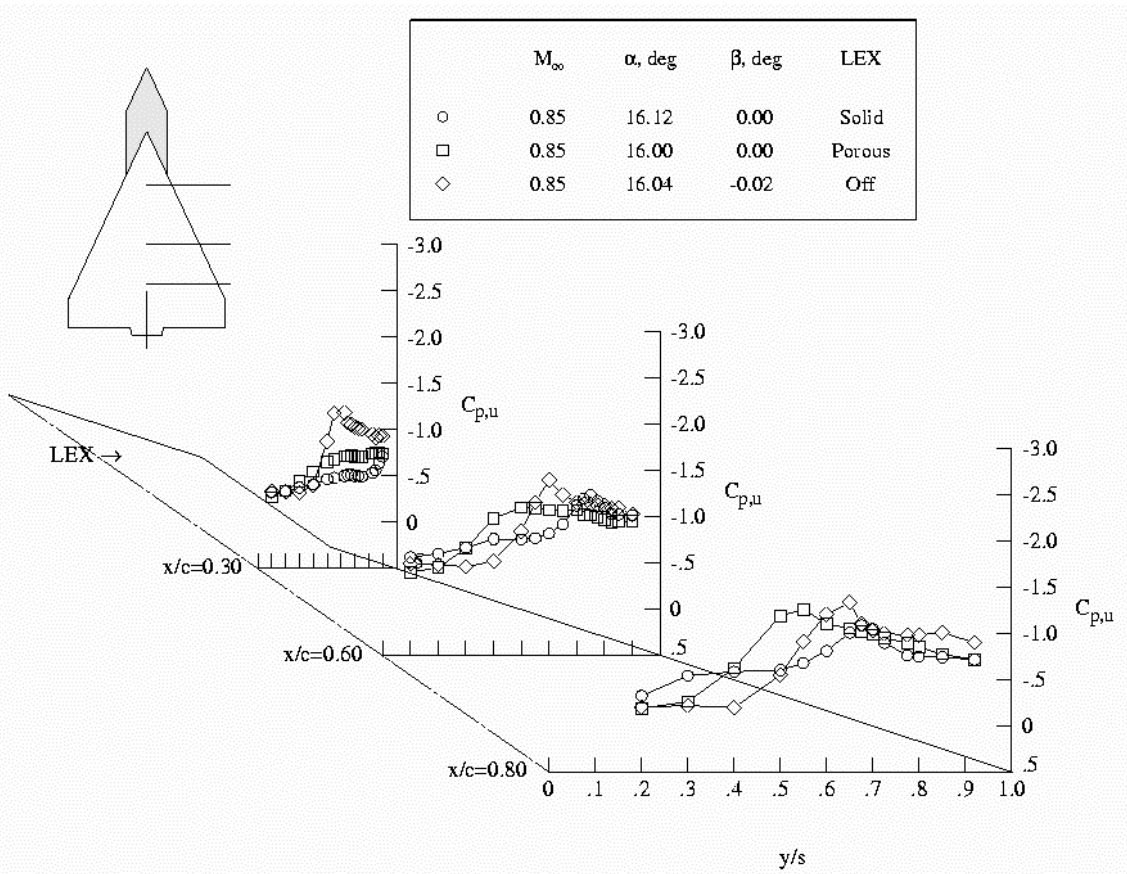


Fig. 10. Spanwise distributions of right wing upper surface static pressure coefficient at $Mach=0.85$, $\alpha=16^\circ$

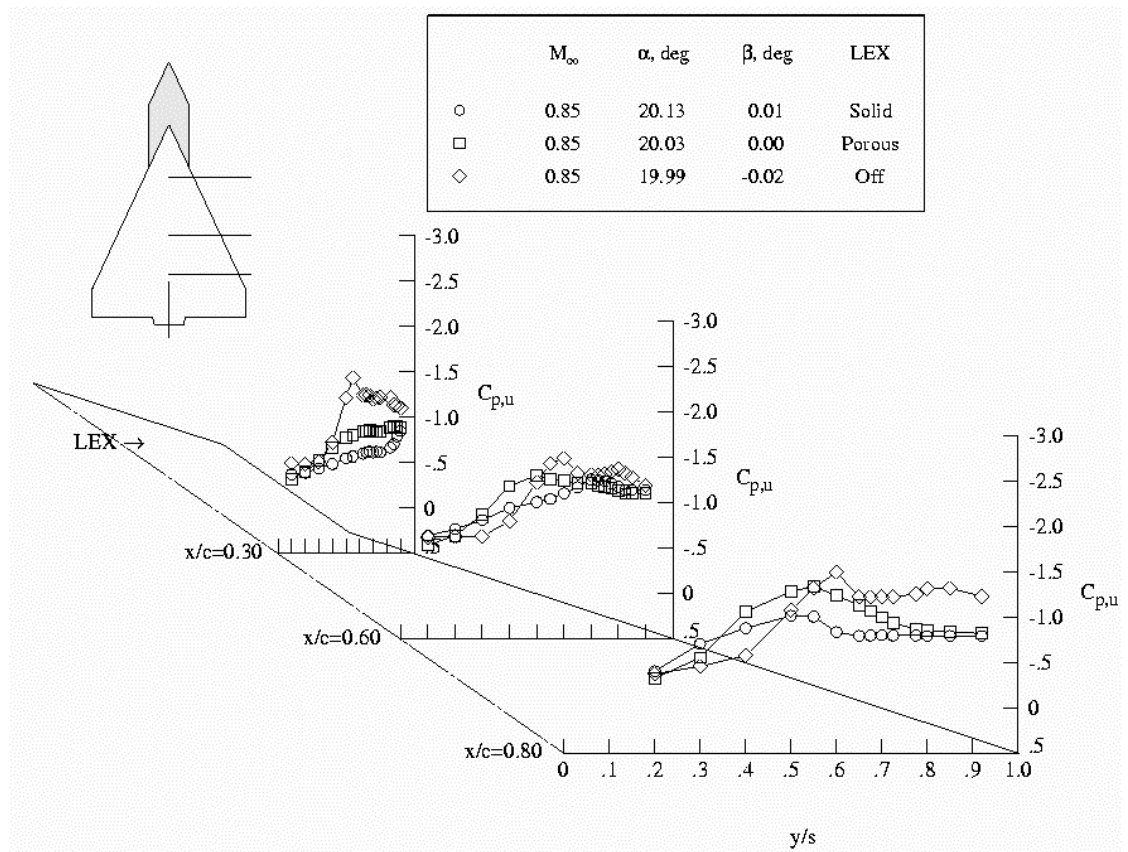


Fig. 11. Spanwise distributions of right wing upper surface static pressure coefficient at $Mach=0.85$, $\alpha=20^\circ$

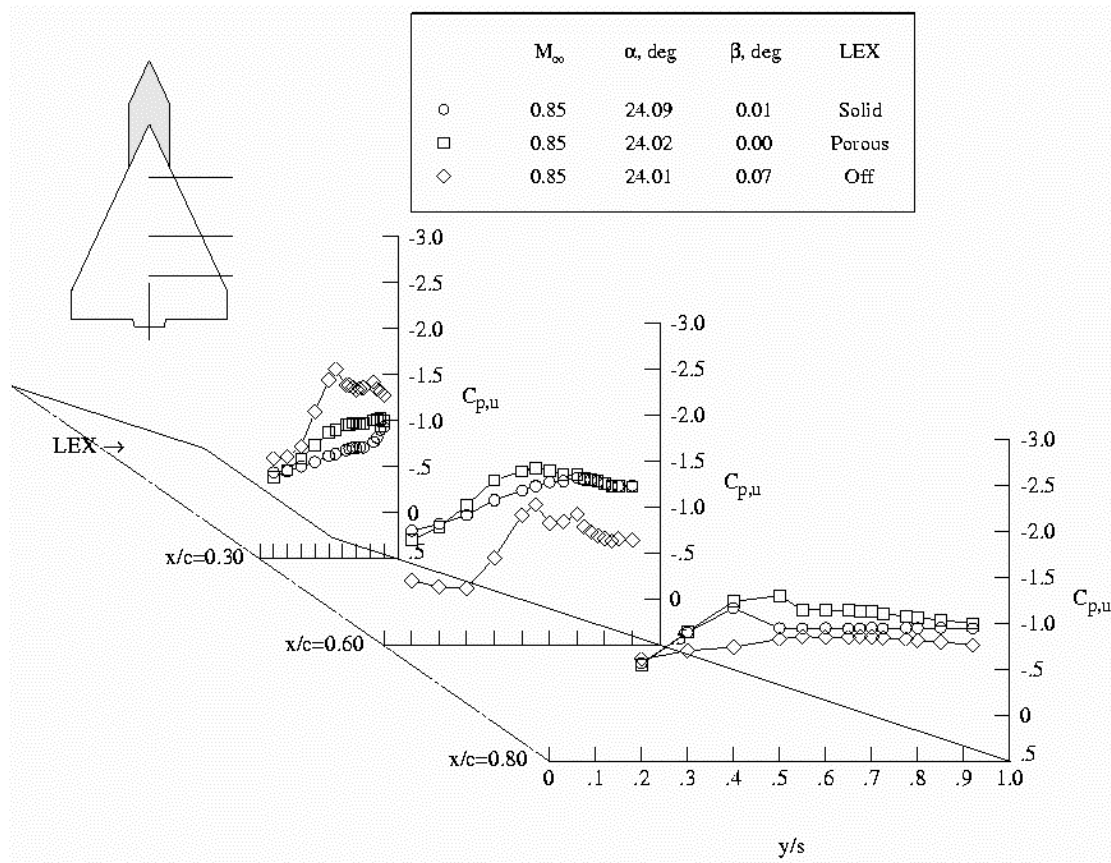


Fig. 12. Spanwise distributions of right wing upper surface static pressure coefficient at $Mach=0.85$, $\alpha=24^\circ$

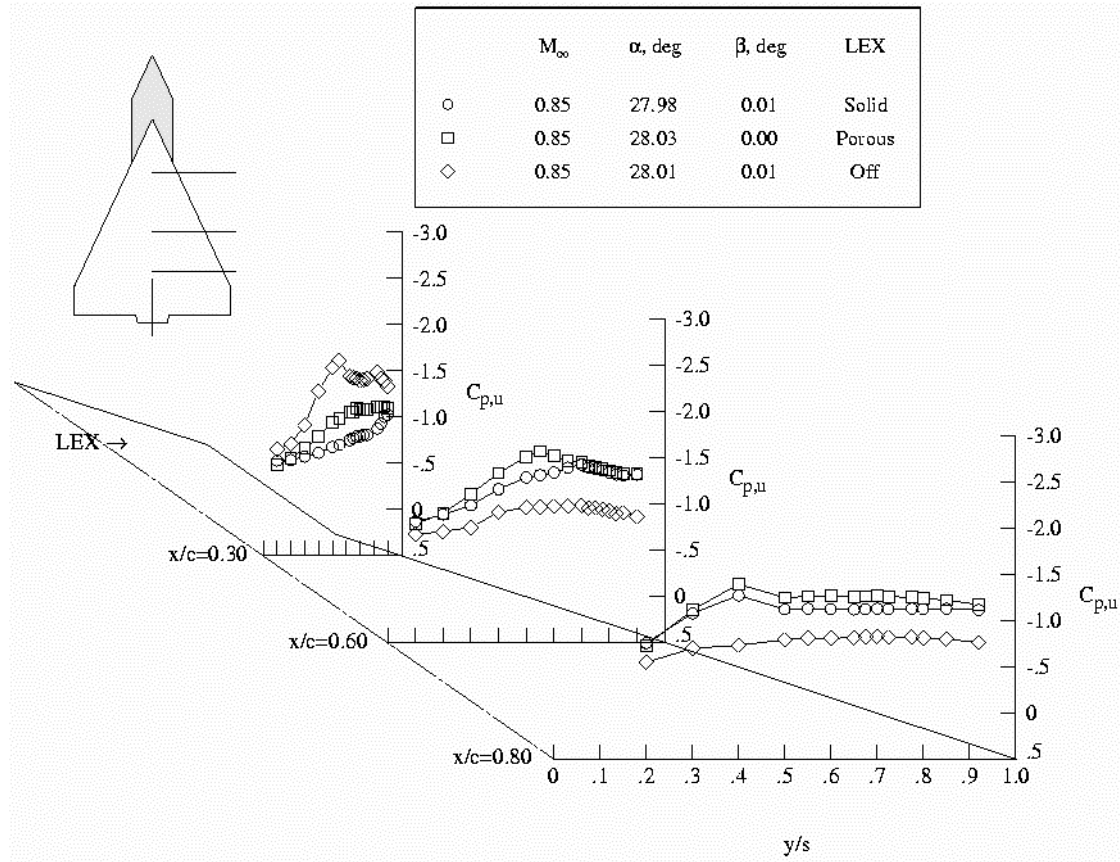


Fig. 13. Spanwise distributions of right wing upper surface static pressure coefficient at $Mach=0.85$, $\alpha=28^\circ$